2

Tsunami dynamics

INTRODUCTION

The approach of a tsunami wave toward shore can be an awesome sight to those who have witnessed it and survived. Figure 2.1 represents an artist's impression of a tsunami wave approaching the coast of Unimak Island, Alaska, early on April 1, 1946. Similar artists' impressions of breaking tsunami will be presented throughout this text. The impressions are accurate. Whereas ordinary storm waves or swells break and dissipate most of their energy in a surf zone, tsunami break at, or surge over, the shoreline. Hence, they lose little energy as they approach a coast and can run up to heights an order of magnitude greater than storm waves. Much of this behavior relates to the fact that tsunami are very long waves—kilometers in length. As shown in Figure 2.1, this behavior also relates to the unusual shape of tsunami wave crests as they approach shore. This chapter describes these unique features of tsunami.

TSUNAMI CHARACTERISTICS

(Wiegel, 1964; Bolt *et al*., 1975; Shepard, 1977; Iida and Iwasaki, 1983; Myles, 1985; von Baeyer, 1999; Ward, 2002)

The terminology used in this text for tsunami waves is shown schematically in Figure 2.2. Much of this terminology is the same as that used for ordinary wind waves. Tsunami have a wavelength, a period, and a deep-water or open-ocean height. They can undergo shoaling, refraction, and diffraction. Most tsunami generated by large earthquakes travel in wave trains containing several large waves that in deep water are less than 0.4 m in height. Figure 2.3 plots typical tidal gauge records or *marigrams* of tsunami at various locations in the Pacific Ocean. These records are taken close to shore and show that tsunami wave heights increase substantially into shallow water. Tsunami wave characteristics are highly variable. In some cases, the waves in a

Figure 2.1. An artist's impression of the tsunami of April 1, 1946 approaching the five story–high Scotch Cap lighthouse, Unimak Island, Alaska. The lighthouse, which was 28 m high, stood on top of a bluff 10 m above sea level. It was completely destroyed (see Figure 2.9). The wave ran over a cliff 32 m high behind the lighthouse. Painting is by Danell Millsap, commissioned by the United States National Weather Service. See color section.

tsunami wave train consist of an initial peak that then tapers off in height exponentially over four to six hours. In other cases, the tsunami wave train consists of a maximum wave peak well back in the wave sequence. The time it takes for a pair of wave crests to pass by a point is termed the wave period. This is a crucial parameter in defining the nature of any wave. Tsunami typically have periods of 100 s–2,000 s (1.6 min–33 min), referred to as the tsunami window. Waves with this period travel at speeds of 600 km h^{-1}–900 km h^{-1} (166 m s^{-1}–250 m s^{-1}) in the deepest part of the

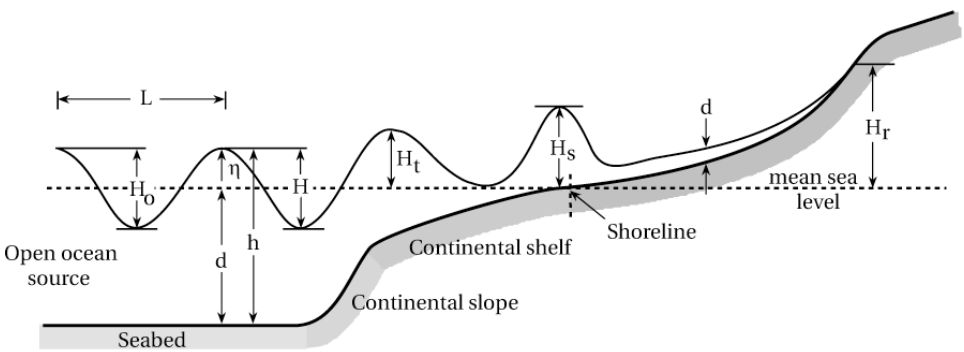

Figure 2.2. Various terms used in the text to express the wave height of a tsunami.

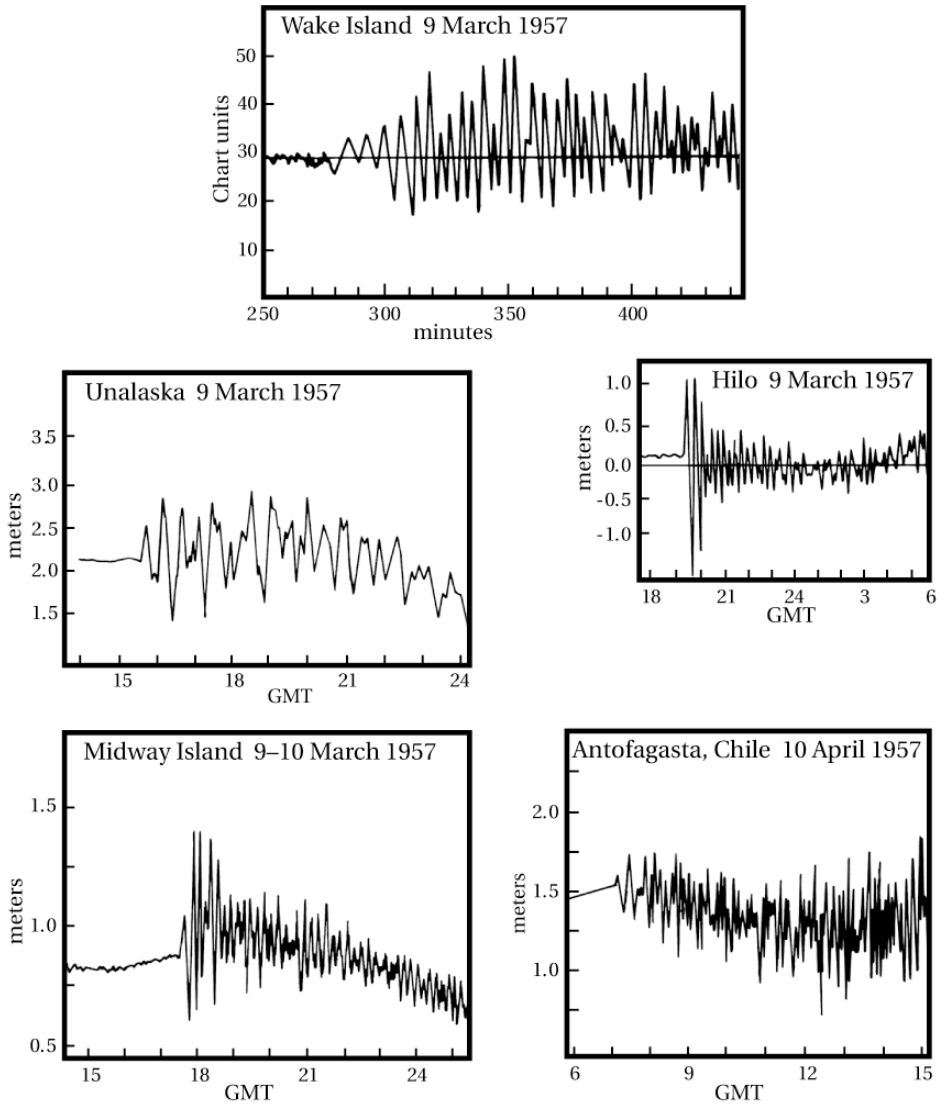

Figure 2.3. Plots or marigrams of tsunami wave trains at various tidal gauges in the Pacific region. Based on Wiegel (1970).

ocean, 100 km h^{-1}–300 km h^{-1} (28 m s^{-1}–83 m s^{-1}) across the continental shelf, and 36 km h^{-1} (10 m s^{-1}) at shore. The upper limit is the speed of a commercial jet airplane. Because of the finite depth of the ocean and the mechanics of wave generation by earthquakes, a tsunami's wavelength—the distance between successive wave crests—lies between 10 km and 500 km. These long wavelengths make tsunami profoundly different from swell or storm waves.

The simplest form of ocean waves is sinusoidal in shape and oscillatory (Figure 2.4). Water particles under oscillatory waves transcribe closed orbits. Hence there is no mass transport of water shoreward with the passage of the wave. Oscillatory waves are described for convenience by three parameters: their height or elevation above the free water surface, their wavelength, and water depth (Figure 2.3). These parameters can be related to each other by three ratios as follows:

$$H : L, \quad H : d, \quad L : d \tag{2.1}$$

where H = crest-to-trough wave height (m)
L = wavelength (m)
d = water depth (m)

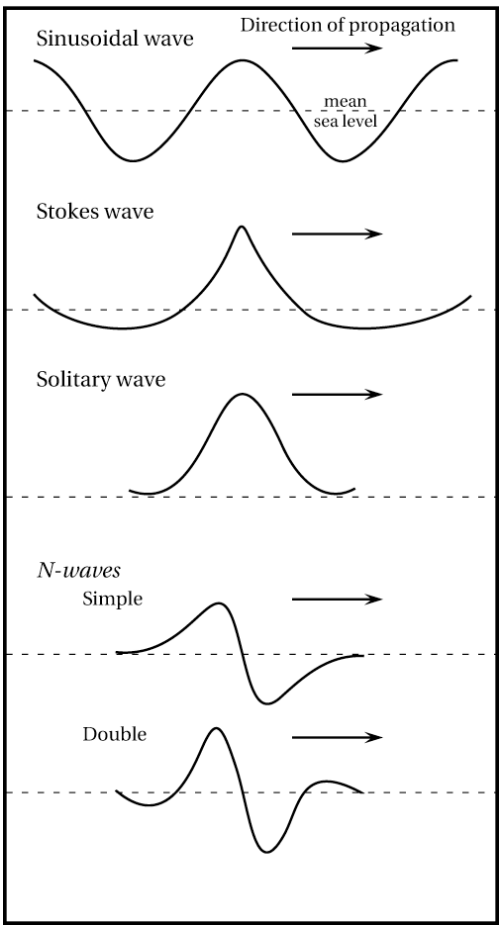

Figure 2.4. Idealized forms characterizing the cross-section of a tsunami wave. Based on Geist (1997b). Note that the vertical dimension is greatly exaggerated.

In deep water, the most significant factor is the ratio $H : L$, or wave steepness. In shallow water it is the ratio $H : d$, or relative height. Sinusoidal waves fit within a class of waves called cnoidal waves: *c* for cosine, *n* for an integer to label the sequence of waves, and *oidal* to show that they are sinusoidal in shape. The shape of a wave or its peakiness can be characterized by a numerical parameter. For sinusoidal waves this parameter is zero. While tsunami in the open ocean are approximately sinusoidal in shape, they become more peaked as they cross the continental shelf. In this case, the numerical parameter describing shape increases and non-linear terms become important. The wave peak sharpens while the trough flattens. These non-linear, tepee-shaped waves are characterized mathematically by Stokes wave theory. In Stokes theory, motion in two dimensions is described by the sum of two sinusoidal components (Figure 2.4). Water particles in a Stokes wave do not follow closed orbits, and there is mass movement of water throughout the water column as the wave passes by a point. As a tsunami wave approaches shore, the separation between the wave crests becomes so large that the trough disappears and only one peak remains. The numerical parameter characterizing shape approaches 1 and the tsunami wave becomes a solitary wave (Figure 2.4). Solitary waves are translatory in that water moves with the crest. All of the waveform also lies above mean sea level. Finally, it has been noted that a trough that is nearly as deep as the crest is high precedes many exceptional tsunami waves. This gives the incoming wave a wall effect. The Great Wave of Kanagawa shown on the frontispiece of this book is of this type. These waves are not solitary because they have a component below mean sea level. Such waveforms are better characterized by *N*-waves. This chapter uses features of each of these wave types: sinusoidal, Stokes, solitary, and *N*-waves to characterize tsunami.

TSUNAMI WAVE THEORY

(Wiegel, 1964, 1970; Okal, 1988; Satake, 1995; Pelinovsky, 1996; Trenhaile, 1997; Komar, 1998)

The form of a sinusoidal wave is analogous to a sine curve (Figure 2.4), and its features can be characterized mathematically by linear, trigonometric functions known as Airy wave theory. This theory can represent local tsunami propagation in water depths greater than 50 m, although in many cases linearity is only violated near the shore, where wave breaking is supposed to occur. In this theory, the three ratios presented in Equation (2.1) are much less than 1. This implies that wave height relative to wavelength is very low—a feature characterizing tsunami in the open ocean. The formulae describing sinusoidal waves vary depending upon the wave being in deep or shallow water. Shallow water begins when the depth of water is less than half the wavelength. As oceans are never more than 5 km deep, the majority of tsunami travel as shallow-water waves. In this case, the trigonometric functions characterizing sinusoidal waves disappear and the velocity of the wave becomes a

simple function of depth as follows:

$$C = (gd)^{0.5} \tag{2.2}$$

where C = wave speed ($\mathrm{m\,s^{-1}}$)
g = gravitational acceleration ($9.81\,\mathrm{m\,s^{-1}}$)

The wavelength of a tsunami is also a simple function of wave speed, C, and period, T, as follows:

$$L = CT \tag{2.3}$$

Equation (2.3) holds for linear, sinusoidal waves and is not appropriate for calculating the wavelength of a tsunami as it moves into shallow water. Linear theory can be used as a first approximation to calculate changes in tsunami wave height as the wave moves across an ocean and undergoes wave shoaling and refraction. The following formulae apply:

$$H = K_r K_s H_o \tag{2.4}$$

$$K_r = (b_o b_i^{-1})^{0.5} \tag{2.5}$$

$$K_s = (d_o d_i^{-1})^{0.25} \tag{2.6}$$

where H_o = crest-to-trough wave height at the source point (m)
K_r = refraction coefficient (dimensionless)
K_s = shoaling coefficient (dimensionless) (Green's Law)
b_o = distance between wave orthogonals at a source point water (m)
b_i = distance between wave orthogonals at any shoreward point (m)
d_o = water depth at a source point (m)
d_i = water depth at any shoreward point (m)

Note that there is a plethora of definitions of wave height in the tsunami literature. These include wave height at the source region, wave height above mean water level, wave height at shore, and wave run-up height above present sea level. The distinctions between these expressions are presented in Figure 2.2. The expression for shoaling—Equation (2.6)—is known as Green's Law. Because tsunami are shallow-water waves, they *feel* the ocean bottom at any depth and their crests undergo refraction or bending around higher seabed topography. The degree of refraction can be measured by constructing a set of equally spaced lines perpendicular to the wave crest. These lines are called wave orthogonals or rays (Figure 2.5). As the wave crest bends around topography, the distance, b, between any two lines will change. Refraction is measured by the ratio $b_o : b_i$. Simple geometry indicates that the ratio $b_o : b_i$ is equivalent to the ratio $\cos \alpha_o : \cos \alpha_i$, where α is the angle that the tsunami wave crest makes to the bottom contours as the wave travels shoreward (Figure 2.5). Once this angle is known, it is possible to determine the angle at any other location using Snell's Law as follows:

$$\sin \alpha_o C_o^{-1} = \sin \alpha_i C_i^{-1} \tag{2.7}$$

where α_o = the angle a wave crest makes to the bottom contours at a source point (degrees)
α_i = the angle a wave crest makes to the bottom contours at any shoreward point (degrees)
C_o = wave speed at a source point ($m\,s^{-1}$)
C_i = wave speed at any shoreward point ($m\,s^{-1}$)

This relationship is straightforward close to shore, but for a tsunami wave crest traveling from a distant source—such as occurs often in the Pacific Ocean—the wave path or ray must also be corrected for geometrical spreading on a spherical surface. Equation (2.4) can be rewritten to incorporate this spreading as follows:

$$H = K_r K_s K_{sp} H_o \tag{2.8}$$

where $K_{sp} = (\sin \Delta)^{-0.5}$
K_{sp} = coefficient of geometrical spreading on a sphere (dimensionless)
Δ = angle of spreading on a sphere relative to a wave's direction of travel

In a large ocean, bathymetric obstacles such as island chains, rises, and seamounts can refract a tsunami wave such that its energy is concentrated or *focused* upon a distant shoreline. These are known as teleseismic tsunami because the effect of the tsunami is translated long distances across an ocean. Japan is particularly prone to tsunami originating from the west coast of the Americas, despite this coastline laying

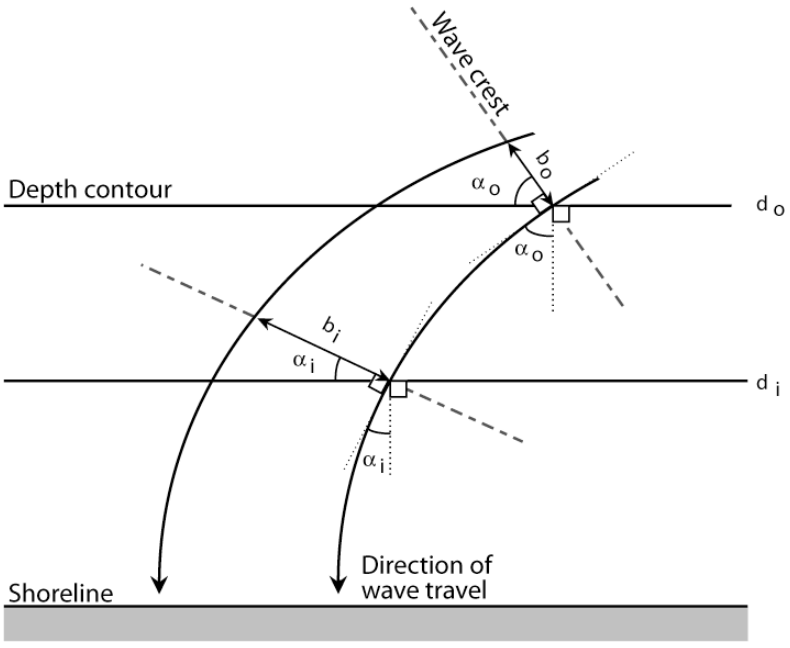

Figure 2.5. Refraction of a tsunami wave crest as it approaches shore.

half a hemisphere away. On the other hand, bottom topography can spread tsunami wave crests, dispersing wave energy over a larger area. This process is called *defocusing*. Tahiti, but not necessarily other parts of French Polynesia, is protected from large tsunami generated around the Pacific Rim because of this latter process.

The measurement of wave height depends upon the location in the ocean where height is measured and the theory that is used to characterize the tsunami wave. For example, solitary wave theory may not be realistic because many observations of tsunami approaching shore note that water is drawn down before the wave crest arrives. This characteristic is due to non-linear effects that produce a trough in front of the wave. Solitons or *N*-waves mimic these features. Wind-generated waves are limited in Stokes wave theory by depth. A Stokes wave will break when the height-to-water depth ratio exceeds 0.78. Tsunami in 75% of cases do not break, but surge onto shore at speeds of $5\,\mathrm{m\,s^{-1}}$–$8\,\mathrm{m\,s^{-1}}$. However, non-linear effects can produce wavelets on the wave crest or in some cases result in the tsunami overriding the shoreline as a bore. Both of these phenomena were observed along coasts during the Indian Ocean Tsunami of 2004. In contrast to storm waves, a tsunami wave is more likely to break on a steeper coast. The popular media often portray this latter aspect as a plunging tsunami wave breaking over the coast. While tsunami crests may have the same energy as storm waves, the two types of waves differ in that storm waves break in a surf zone and dissipate most of their energy before reaching shore. On the other hand, tsunami reach shore usually without breaking and bring tremendous power to bear on the coastline (Figure 2.6).

◄ **Figure 2.6.** Sequential photographs of the March 9, 1957 tsunami overriding the backshore at Laie Point on the Island of Oahu, Hawaii. An earthquake in the Aleutian Islands 3,600 km away, with a surface magnitude of 8.3, generated the tsunami. Photograph Credit: Henry Helbush. *Source:* United States Geological Survey, Catalogue of Disasters # B57C09-002.

Resonance

(Wiegel, 1964, 1970)

Tsunami, having long periods of 100 s–2,000 s, can also be excited or amplified in height within harbors and bays if their period approximates some harmonic of the natural frequency of the basin. The term *tsunami* in Japanese literally means "harbor wave" because of this phenomenon. Here tsunami can oscillate back and forth for 24 hours or more. The oscillations are termed *seiches*, a German word used to describe long, atmospherically induced waves in Swiss alpine lakes. Seiches are independent of the forcing mechanism and are related simply to the 3-dimensional form of the bay or harbor as follows:

$$\text{Closed basin:} \quad T_s = 2L_b(gd)^{-0.5} \tag{2.9}$$

$$\text{Open basin:} \quad T_s = 4L_b(gd)^{-0.5} \tag{2.10}$$

where L_b = length of a basin or harbor (m)
T_s = wave period of seiching in a bay, basin, or harbor(s)

Equation (2.9) is appropriate for enclosed basins and is known as Merian's Formula. In this case, the forcing mechanism need have no link to the open ocean. As an example, an Olympic-sized swimming pool measuring 50 m long and 2 m deep would have a natural resonance period of 22.6 s. Any vibration with a periodicity of 5.6 s, 11.3 s, and 22.6 s could induce water motion back and forth along the length of the pool. If sustained, the oscillations or seiching would increase in amplitude and water could spill out of the pool. Seismic waves from earthquakes can provide the energy for seiching in swimming pools, and the Northridge earthquake of January 17, 1994 was very effective at emptying pools in Los Angeles. Seiching was also induced in bays in Texas and the Great Lakes of North America about 30 minutes after the Great Alaskan Earthquake of 1964. Volcano-induced, atmospheric pressure waves can generate seiching as well. The eruption of Krakatau in 1883 produced a 0.5 m high seiche in Lake Taupo in the middle of the North Island of New Zealand via this process. Whether or not either of these phenomena technically is a tsunami is a moot point.

Resonance can also occur in any semi-enclosed body of water with the forcing mechanism being a sudden change in barometric pressure, semi- or diurnal tides, and tsunami. In these cases the wave period of the forcing mechanism determines whether the semi-enclosed body of water will undergo excitation. The effects can be quite dramatic. For example, the Bay of Fundy, on the east coast of Canada, has a resonance period that is within 6 minutes of the diurnal tidal period of 12.42 hours. One-meter high tides in the open ocean are amplified to 14 m within the bay, while atmospheric pressure disturbances during storms moving up the coast can generate storm surges equal to another 16 m. Tsunami have the same potential. The predominant wave period of the tsunami that hit Hawaii on April 1, 1946 was 15 minutes. The tsunami was most devastating around Hilo Bay, which has a critical resonant length of about 30 minutes. While most tsunami usually approach a coastline parallel to shore, those in Hilo Bay often run obliquely alongshore because of resonance and

edge-wave formation. Damage in Hilo due to tsunami has always been a combination of the tsunami and a tsunami-generated seiche. The above treatment of resonance is cursory. Harbor widths can also affect seiching and it is possible to generate subharmonics of the main resonant period that can complicate tsunami behavior in any harbor or bay. These aspects are beyond the scope of this text.

Shallow-water, long-wave theory

(Mader, 1974, 1988; Murty, 1977, 1984; Titov and González, 1997)

The preceding theories model either small-amplitude or long waves. They cannot do both at same time. Tsunami behave as small-amplitude, long waves. Their height-to-length ratio may be higher than 1:100,000. If tsunami are modeled simply as long waves, they become too steep as they shoal toward shore and break too early. This is called the long-wave paradox. About 75% of tsunami do not break during run-up. Because their relative height is so low, tsunami are also very shallow waves. Under these conditions, tsunami characteristics can be modeled more realistically by using incompressible, shallow-water long-wave equations in which depth is small compared with the tsunami's wavelength. In their simplest form, vertical velocity components under the wave are assumed negligible.

Shallow-water, long-wave equations are solved using non-linear, finite-difference techniques. A grid is placed over a study area, and height and velocity values are calculated over time across the grid using depths interpolated at either the center or corners of the grid. A simple grid is shown in Figure 2.7. Problems of grid interpolation immediately become obvious. The ocean's depths are not measured on a regular grid, and depths must be interpolated from survey lines that crisscross an ocean. The density of these survey lines is not constant, but increases shoreward. Error in interpolation always exists using these survey values. For example, in Figure 2.7 on the cell marked B, the elevation in the bottom right-hand corner is clearly close to 10 m. However, in the top right-hand corner, the depth value is less obvious. Interpolation at this latter point can be performed objectively using spline or polynomial fitting techniques, but a degree of error will always exist. In deep water, depths vary little and the effect of changing bathymetry upon a tsunami is minimal. However, in shallower water, increases in topographic variability affect behavior more. Once a long wave crosses the shelf, its behavior is influenced by both longshore and onshore variations in topography. As a rule of thumb, there should be 30 grid points covering the wavelength of a tsunami wave. For a tsunami with a wave period of 5 minutes, this criterion requires grid sizes of 50 m, 100 m, and 500 m where the depth of water exceeds 2.5 m, 10 m, and 250 m, respectively. Accurate depth information is more important than the width of the grid in modeling tsunami behavior precisely in the nearshore zone. Calculations can also be performed using triangular grid cells. The size of the triangles decreases toward shore. More advanced modeling techniques can accommodate variable grid sizes. In recent years, with the demise of the Cold War, this type of detailed bathymetry has become available in the open ocean; however, inshore bathymetry is not as accessible because it usually comes under the domain of individual countries.

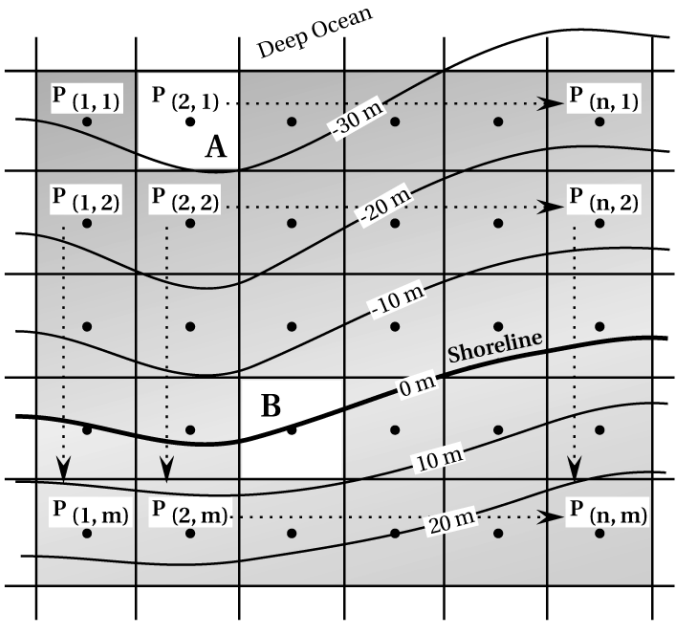

Figure 2.7. Simple representation of gridded bathymetry. Interpolation of depth values occurs at the center of grid cells—as in this figure—or at the grid intersects. Computer simulations of actual tsunami use grids of much higher resolution than presented here.

One of the most common computer programs solving shallow-water long-wave equations is the SWAN code, developed by Charles Mader in the mid-1970s. In this procedure, a tsunami wave is not traced iteratively into shore; rather, changes in water level are calculated simultaneously across the whole depth grid iteratively over time. The technique is ideal for determining the amount of reflection of tsunami wave energy from a slope or the behavior of a tsunami wave in an enclosed bay or harbor. It is also possible to add any wave generated by aftershocks to the calculations. Finally, the method mimics the withdrawal and subsequent flooding of a coast over time as a tsunami wave approaches shore. The stability of solutions is a crucial function of the time increment used in the calculations. The modeling becomes unstable at time increments of less than 4 seconds. For a 10-minute period tsunami wave, crossing a shelf 100 km wide, the shallow-water long-wave equations can only be solved using supercomputers. An example of shallow-water, long-wave techniques is shown in Figure 2.8 for the June 10, 1996 Andreanov earthquake originating from the Aleutian Islands in the North Pacific Ocean. Only the first three or four waves in the train are shown, and nowhere does wave height exceed 50 cm. An extensive array of tide gauges and buoys showed that heights and arrival times were well simulated in this model. Accurate solutions for tsunami wave trains can now be performed within hours of the occurrence of any major earthquake, using similar simulations. Real-time modeling is not yet possible.

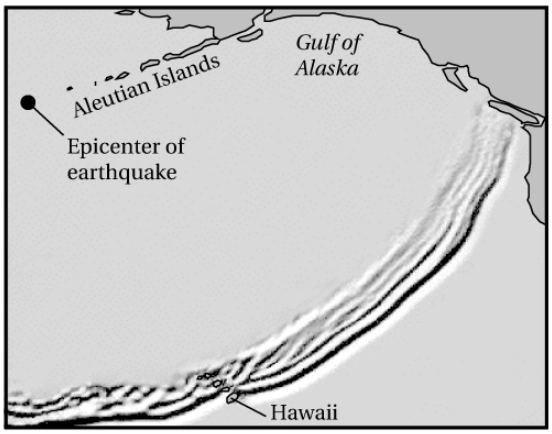

Figure 2.8. Computer simulation of the tsunami wave train generated by the 10 June 1996 Andreanov earthquake on the tip of the Alaskan Peninsula. The simulation uses shallow-water, long-wave equations (Titov and González, 1997). For presentation purposes, the complex reflected wave crests behind the main wave front have been removed. Wave height nowhere exceeds fifty centimeters.

The shallow-water long-wave equations work well in the open ocean, on continent slopes, around islands, and in harbors. On a steep continental slope greater than 4°, the techniques show that a tsunami wave will be amplified by a factor of 3 to 4 times. Because they incorporate both flooding and frictional dissipation, the equations overcome problems with linear theory where the wave breaks too far from shore. They also show that, because of reflection, the second and third waves in a tsunami wave train can be amplified as the first wave in the train interacts with shelf topography. The shallow-water long-wave equations do have limitations. If they do not include vertical velocity components, they cannot describe wave motion resulting from the formation of cavities in the ocean surface (asteroid impacts); replicate wave profiles generated by sea floor displacement, underwater landslides, or tsunami traveling over submerged barriers; or simulate the behavior of short-wavelength tsunami. They still suffer in some cases from the long-wave paradox and break too early. In these cases, incompressible, shallow-water long-wave equations must be used that include the vertical components of motion. This increases the total computation time; however, more complicated situations can be modeled more accurately. For example, the effect of tsunami crossing reefs or underwater barriers can be simulated. Effectively, an underwater barrier does not become significant in attenuating the tsunami wave height until the barrier height is more than 50% the water depth. Even where the height of this barrier is 90% of the water depth, half of the tsunami wave height can be transmitted across it. Modeling using the full shallow-water, long-wave equations shows that submerged offshore reefs do not necessarily protect a coast from the effects of tsunami. This is important because it indicates that a barrier such as the Great Barrier Reef of Australia may not protect the mainland coast from tsunami.

RUN-UP AND INUNDATION

Run-up

(Wiegel, 1964, 1970; Yeh, 1991; Camfield, 1994; Yeh *et al*., 1994; Briggs *et al*., 1995; Geist, 1977b)

Tsunami are known for their dramatic run-up heights, which commonly are greater than the height of the tsunami approaching shore by a factor of 2 or more times. For example, in the Pacific Ocean region, 41 tsunami have generated wave run-up heights in excess of 6 m since 1900, while five events since 1600 have produced run-up heights between 51 m and 115mm. The March 26, 1947 earthquake offshore from Gisborne, New Zealand, generated a 10 m high run-up. Such high run-ups are usually localized; however, this value was maintained along a 13 km stretch of coast. The Alaskan tsunami of April 1, 1946 overtopped cliffs on Unimak Island and wiped out a radio mast standing 35 m above sea level (Figure 2.9). The eruption of Krakatau in 1883 generated a wave that reached elevations up to 40 m high along the surrounding

Figure 2.9. The remains of the Scotch Cap lighthouse, Unimak Island, Alaska, following the April 1, 1946 tsunami. A Coast Guard station, situated at the top of the cliff 32 m above sea level, was also destroyed. Five men in the lighthouse at the time perished. *Source:* United States Department of Commerce, National Geophysical Data Center.

coastline. By far the largest run-up height recorded was that produced on July 9, 1958 by an earthquake-triggered landslide in Lituya Bay, Alaska. Water swept 524 m above sea level up the slope on the opposite side of the bay, and a 30 m to 50 m high tsunami propagated down the bay. In Japan, run-up heights as high as 38.2 m have been measured. The 1896 earthquake offshore from the Sanriku coast sent a wave this high crashing into the towns of Yoshihama and Kamaishi.

Tsunami differ from wind-generated waves in that significant water motion occurs throughout the whole water column. While this may not be important on the shelf, it causes the tsunami to take on the shape of a solitary wave in shallow water. A solitary wave maintains its form in shallow water, and, because the kinetic energy of the tsunami is evenly distributed throughout the water column, little energy is dissipated, especially on steep coasts. The maximum run-up height of a solitary wave can be approximated using the following formula:

$$H_{r\max} = 2.83(\cot \beta)^{0.5} H_t^{1.25} \tag{2.11}$$

where $H_{r\max}$ = maximum run-up height of a tsunami above sea level (m)
H_t = wave height at shore or the toe of a beach (m)
β = slope of the seabed (degrees)

The run-ups derived from Equation (2.11) are higher than those predicted using sinusoidal waves. If a leading trough precedes the tsunami, then its form is best characterized by an *N*-wave (Figure 2.4). These waves are more likely to be generated close to shore because the critical distance over which a tsunami wave develops is not long enough relative to the tsunami's wavelength to generate a wave with a leading crest. This critical distance may be as great as 100 km from shore—a value that encompasses many near-coastal tsunamigenic earthquakes. *N*-waves, as shown in Figure 2.4, can take on two forms: simple and double. The double wave is preceded by a smaller wave. The tsunami generated by the Indian Ocean Tsunami along the south Sri Lankan coast was a double *N*-wave. Run-ups for *N*-waves can be approximated by the following formulae:

$$\text{Simple } N\text{-wave} \quad H_{r\max} = 3.86(\cot \beta)^{0.5} H_t^{1.25} \tag{2.12}$$

$$\text{Double } N\text{-wave} \quad H_{r\max} = 4.55(\cot \beta)^{0.5} H_t^{1.25} \tag{2.13}$$

The two equations are similar in form to Equation (2.11) for solitary waves. However, they result in run-ups that are 36% and 62% higher. In some cases, *N*-waves may account for the large run-ups produced by small earthquakes. For example, an earthquake (M_s magnitude of 7.3) struck the island of Pentecost, Vanuatu, on November 26, 1999. Normally, an event of this magnitude would generate only a minor tsunami, if one at all. Instead, run-up reached 5 m above sea level. The tsunami was characterized by a distinct leading depression.

The run-up height of a tsunami also depends upon the configuration of the shore, diffraction, standing wave resonance, the generation of edge waves that run at right angles to the shoreline, the trapping of incident wave energy by refraction of reflected waves from the coast, and the formation of Mach–Stem waves. Mach–Stem waves

are not a well-recognized feature in coastal dynamics. They have their origin in the study of flow dynamics along the edge of airplane wings, where energy tends to accumulate at the boundary between the wing and air flowing past it. In the coastal zone, Mach–Stem waves develop wherever the angle between the wave crest and a cliff face is greater than 70°. The portion of the wave nearest the cliff continues to grow in amplitude even if the cliff line curves back from the ocean. The Mach–Stem wave process is insensitive to irregularities in the cliff face. It can increase ocean swell by a factor of 4 times. The process often accounts for fishermen being swept off rock platforms during rough seas. The process explains how cliffs 30 m or more in height can be overtopped by a shoaling tsunami wave that produces run-up reaching only one-third as high elsewhere along the coast. Mach–Stem waves play a significant role in the generation of high-speed vortices responsible for bedrock sculpturing by large tsunami—a process that will be described in the following chapter.

All these processes, except Mach–Stem waves, are sensitive to changes in shoreline geometry. This variability accounts for the wide variation in tsunami wave heights over short distances. Within some embayments, it takes several waves to build up peak tsunami wave heights. Figure 2.10 maps the run-up heights around Hawaii for the Alaskan tsunami of April 1, 1946. The northern coastline facing the tsunami received the highest run-up. However, there was also a tendency for waves to wrap around the islands and reach higher run-ups at supposedly protected sites, especially on the islands of Kauai and Hawaii. Because of refraction effects, almost every promontory also experienced large run-ups, often more than 5 m high. Steep coastlines were hardest hit because the tsunami waves could approach shore with

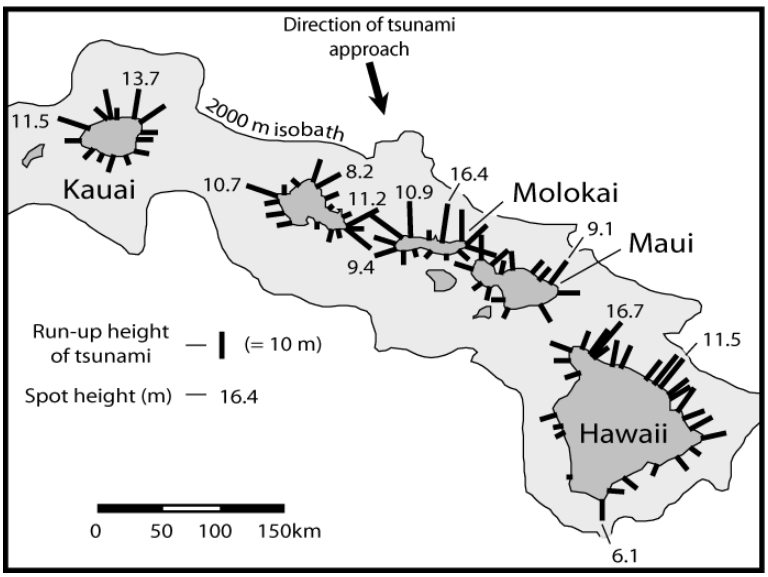

Figure 2.10. Run-up heights around the Hawaiian Islands for the Alaskan tsunami of April 1, 1946. Based on Shepard (1977).

Figure 2.11. The American warship *Wateree* in the foreground and the Peruvian warship *America* in the background. Both ships were carried inland 3 km by a 21 m high tsunami wave during the Arica, South American event of August 13, 1868. Retreat of the sea from the coast preceded the wave, bottoming both boats. The *Wateree,* being flat hulled, bottomed upright and then surfed the crest of the tsunami wave. The *America,* being keel-shaped, was rolled repeatedly by the tsunami. Photograph courtesy of the United States Geological Survey. *Source:* Catalogue of Disasters # A68H08-002.

minimal energy dissipation. For all of these reasons, run-up heights were spatially very variable. In some places—for example, on the north shore of Molokai—heights exceeded 10 m, while several kilometers away they did not exceed 2.5 m.

Tsunami interaction with inshore topography also explains why larger waves often appear later in a tsunami wave train. For example, during the 1868 tsunami off Arica, South America, the *USS Wateree* and the Peruvian ship *America* escaped the first two waves, but were picked up by a third wave 21 m high. The wave moved the two ships 5 km up the coast and 3 km inland, overtopping sand dunes (Figure 2.11). The ships came to rest at the foot of the coastal range, where run-up had surged to a height 14 m above sea level. Similarly, during the April 1, 1946 tsunami that devastated Hilo, Hawaii (the same tsunami that destroyed the Scotch Cap lighthouse shown in Figures 2.1 and 2.9), many people were killed by the third wave, which was much higher than the preceding two.

Shallow-water long-wave equations can accurately simulate run-up. Figure 2.12 presents the results for a tsunami originally 3 m high with a period of 900 seconds traveling across a shelf of 12 m depth onto a beach of 1% slope. Under these conditions, linear theory would have the wave breaking several kilometers from shore. However, the shallow-water long-wave equations indicate that the wave surges onto the beach with a wave front that is 3.5 m high. This is similar to many descriptions of

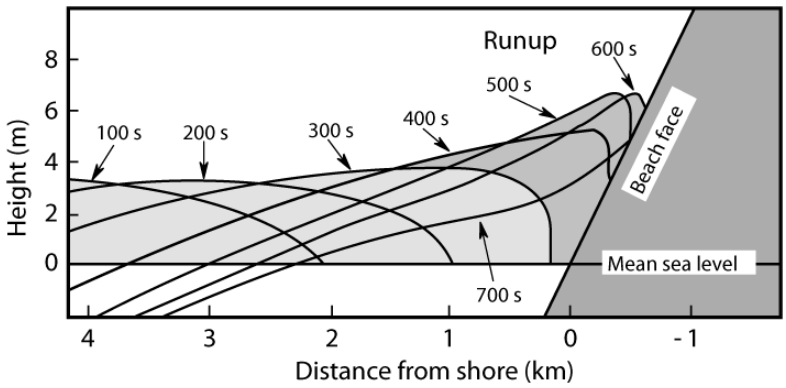

Figure 2.12. Run-up of a tsunami wave onto a beach modeled using shallow-water, long-wave equations. The model used a grid spacing of 10 and 0.5 s time increments. The original sinusoidal wave had a height of 3 m and a period of 900 s. Run-up peaked at 6 m above mean sea level and penetrated 600 m inland on a 1% slope. Based on Mader (1990).

tsunami approaching shallow coasts, especially the one that approached the coast of Thailand during the Indian Ocean Tsunami event. While flooding can occur long distances inland, the velocity of the wave front can slow dramatically. During the Oaxaca, Mexico, Tsunami of October 9, 1995, people were able to outrun the wave as it progressed inland. A tsunami's backwash can be just as fast as, if not faster than, its run-up. The modeled wave shown in Figure 2.12 took 300 seconds to reach its most shoreward point, but just over 100 seconds to retreat from the coast. Tsunami backwash is potentially just as dangerous as run-up. Unfortunately, little work has been done on tsunami backwash.

The sheltered locations on the lee side of islands appear particularly vulnerable to tsunami run-up. Solitary waves propagate easily along steep shores, forming a trapped edge wave. Laboratory models show that the maximum run-up height of this trapped wave is greatest toward the rear of an island. More important, the run-up velocity here can be up to three times faster than at the front. For example, the December 12, 1992 tsunami along the north coast of Flores Island, Indonesia, devastated two villages in the lee of Babi, a small coastal island lying 5 km offshore. Run-up having maximum heights of 5.6 m–7.1 m completely destroyed two villages and killed 2,200 people. Similarly, during the July 12, 1993 tsunami in the Sea of Japan, the town of Hamatsumae, lying behind the island of Okusihir, was destroyed by a 30 m high tsunami run-up that killed 330 people.

Finally, tsunami run-up can also take on complex forms. Video images of tsunami waves approaching shore show that some decay into one or more bores. A bore is a special waveform in which the mass of water propagates shoreward with the wave. The leading edge of the wave is often turbulent. Waves in very shallow water can also break down into multiple bores or solitons. Soliton formation can be witnessed on many beaches where wind-generated waves cross a shallow shoal, particularly at low tide. Such waves are paradoxical because bores should dissipate

their energy rapidly through turbulence and frictional attenuation, especially on dry land. However, tsunami bores are particularly damaging as they cross a shoreline. Detailed analysis indicates that the bore pushes a small wedge-shaped body of water shoreward as it approaches the shoreline. This transfers momentum to the wedge, increasing water velocity and turbulence by a factor of 2. While there is a rapid decrease in velocity inland, material in the zone of turbulence can be subject to impact forces greater than those produced by ordinary waves. Often objects can travel so fast that they become water-borne missiles. This process can also transport a large amount of beach sediment inland. Tsunami that degenerate into bores are thus particularly effective in sweeping debris inland.

Inland penetration

(Hills and Mader, 1997)

As a rough rule of thumb, the cross-sectional area of coastline flooded by a tsunami is equal to the cross-sectional area of water under the wave crest close to shore. This effect is illustrated by Figure 2.13. The bigger the tsunami, or the longer its wave period, the greater the volume of water carried onshore and the greater the extent of flooding. The maximum distance that run-up can penetrate inland on a flat coast can be calculated using the following formula:

$$x_{\max} = (H_t)^{1.33} n^{-2} k \tag{2.14}$$

where $x_{\max}$ = limit of landward incursion (m)
n = Manning's n
k = a constant

Very smooth terrain such as mud flats or pastures has a Manning's n of 0.015. Areas covered in buildings have a value of 0.03, and densely treed landscapes have a value of

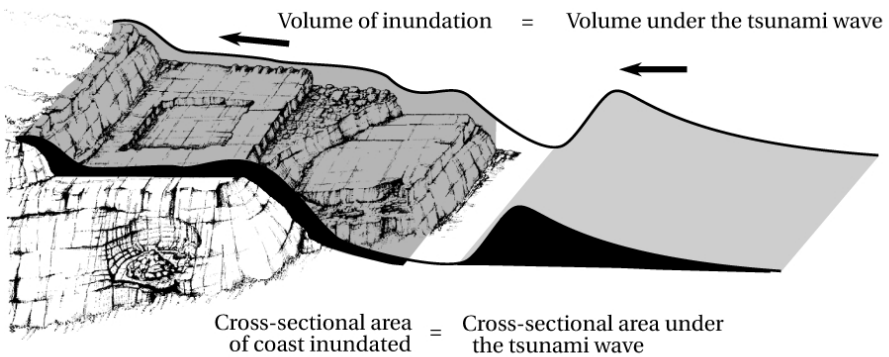

Figure 2.13. Schematic diagram showing that the cross-sectional area of coastline flooded, and volume of inundation by a tsunami is equal to the cross-sectional area and volume of water under the tsunami wave crest. The landscape represented in this diagram will be described in Chapter 4.

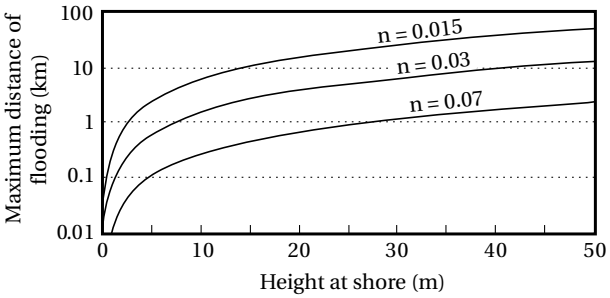

Figure 2.14. Tsunami height vs. landward limit of flooding on a flat coastal plain of varying roughness. Roughness is represented by Manning's n, where n equals 0.015 for very smooth topography, 0.03 for developed land, and 0.07 for a densely treed landscape. Based on Hills and Mader (1997).

0.07. The constant in Equation (2.14) has been evaluated for many tsunami and has a value of 0.06. The equation assumes that the run-up height equals the maximum depth of the tsunami at shore. Using this value, the maximum distance that tsunami can flood inland is plotted in Figure 2.14 for different run-up heights, for the three values of Manning's n mentioned. For developed land on flat coastal plains, a tsunami with a height of 10 m at shore can penetrate 1.4 km inland. Exceptional tsunami with heights at shore of 40 m–50 m can race 9 km–12 km inland. Only large earthquakes, submarine landslides, and asteroid impacts with the ocean can generate these latter wave heights. For crops or pasture, the same waves could theoretically rush inland four times farther—distances of 5.8 km for a 10 m high wave at shore and 36 km–49 km for the 40 m to 50 m high tsunami. The Indian Ocean Tsunami at Banda Aceh, Indonesia in 2004 with a height of 10 m at shore reached these predicted limits, traveling 5 km inland. Equation (2.14) also indicates that the effect of a tsunami can be minimized on flat coastal plains by planting dense stands of trees. For example, a 10 m high tsunami can only penetrate 260 m inland across a forested coastal plain, while extreme waves 40 m–50 m in height could not travel more than 2.3 km inland across the same terrain.

Depth and velocity at shore

(Blong, 1984; Camfield, 1994; Yeh *et al.*, 1994; Nott, 1997)

Equation (2.2) indicates that the velocity of a tsunami wave is solely a function of water depth. Once a tsunami wave reaches dry land, then wave height equates with water depth and the following equations apply:

$$H_t = d \tag{2.15}$$

$$v_r = 2(gH_t)^{0.5} \tag{2.16}$$

where v_r = velocity of run-up ($\mathrm{m\,s^{-1}}$)
d = the depth of water flow over land (m)

This equation yields velocities of $8\,m\,s^{-1}$–$9\,m\,s^{-1}$ for a 2 m high tsunami wave at shore. Slope and bed roughness can be incorporated into the calculation as follows:

$$v_r = H_t^{0.7}[\tan(\beta_w)]^{0.5} n^{-1} \tag{2.17}$$

where β_w = slope of the water surface (degrees)

While the inclination of the water surface can be a difficult parameter to estimate, it can be determined after an event by measuring water lines on buildings and trees, and debris left stranded in vegetation. Generally, the inclination of the water surface ranges between 0.001 and 0.0025, increasing with slope. In Japan, it has been shown that for a Manning's n of 0.023, velocities under a tsunami wave can range between $1.3\,m\,s^{-1}$ and $5.6\,m\,s^{-1}$ using Equation (2.17). In Hilo, Hawaii, the 8 m high tsunami of 1946 mentioned earlier could have obtained velocities between $5.9\,m\,s^{-1}$ and $9.3\,m\,s^{-1}$—far faster than people could run. Where tsunami behave as solitary waves and encircle steep islands, velocities in the lee of the island have been found to be three times higher than those calculated using this equation.

The velocities defined by Equations (2.16) and (2.17) have the potential to move sediment and erode bedrock, producing geomorphic features in the coastal landscape that uniquely define the present of both present-day and past tsunami events. These signatures will be described in detail in the following chapter.